Toward Astrometric Tracking With the Infrared Spatial Interferometer

R. N. Treuhaft
Radar Science and Engineering Section

M. Bester, W. C. Danchi, and C. H. Townes
Space Sciences Laboratory, University of California at Berkeley

Infrared interferometric demonstrations with the University of California, Berkeley's infrared spatial interferometer (ISI) on Mt. Wilson explore the potential of infrared and optical astrometry for deep space tracking, reference frame development, and DSN science. Astrometric data taken and analyzed over the last 5 years from the ISI have shown that instrumental and atmospheric effects limit current demonstrations. The benefits of sensitivity upgrades, which were performed in 1991 and 1992, have been demonstrated by comparing point-to-point phase fluctuations for the fall 1989 and fall 1992 observing epochs. This comparison showed that point-to-point phase fluctuations due to tropospheric and quantum noise, for optimal integration times of 0.2 sec, are approaching the 0.1-cycle level needed to reliably connect the interferometric phase. The increase in sensitivity, coupled with that arising from very recent hardware upgrades, will greatly enhance phase-connection capabilities necessary for astrometry in the presence of atmospheric refractivity fluctuations. The current data set suggests that atmospheric fluctuations on Mt. Wilson during the best seeing are dominated by a low-lying component, approximately 25 m high, which may be minimized with in situ calibration in the future. During poor seeing conditions that currently prohibit the interferometric phase connection necessary for astrometry, fluctuations seem to be generated by atmospheric inhomogeneities at much higher altitudes above Mt. Wilson. Data taken over the last year suggest that the ISI will soon be able to achieve 50- to 100-nrad astrometry in a single observing session, employing current ground-based laser distance interferometer calibrations to minimize atmospheric effects.

I. Introduction

Infrared and optical astrometry support three areas of potential interest to the Deep Space Network (DSN): tracking of laser-carrying spacecraft; reference frame development, including locating solar system objects in infrared/optical, radio, and planetary reference frames; and DSN astrometric science of the future. Because optical telemetry is being considered for high data-rate transmission within the next few decades [1], development of

an infrared or optical metric tracking capability will reduce or eliminate the need for bulky radio equipment on laser-carrying spacecraft. Even in the absence of optical telemetry, the development of infrared and optical reference frames, and the location of solar system objects in those frames, will enable more accurate target-relative tracking with radio systems utilizing radio-optical frame ties. Optical measurements of Global Positioning System (GPS) satellites constitute one example of a radio-optical frame-tie technique. Such measurements are planned for the Table Mountain Ronchi telescope in the near future. Current DSN science frequently involves the measurement of electromagnetic phase or amplitude at radio wavelengths. Similar measurements at infrared and optical wavelengths—such as solar deflection experiments, free of charged-particle effects, and asteroid imaging—will probably be performed by the DSN of the future.

Stellar astrometric demonstrations with the University of California, Berkeley's infrared spatial interferometer (ISI) bear on each of the three areas of DSN interest mentioned above. ISI astrometric demonstrations, which help to determine the limiting accuracy of ground-based infrared or optical astrometry, provide a valuable assessment of the limiting accuracy of tracking, reference frame work, and science at infrared and optical wavelengths. For example, atmospheric refractivity fluctuations studied with ISI are likely to be the dominant astrometric error for tracking spacecraft, galactic, or solar system targets. Refractivity fluctuations are similar in spatiotemporal characteristics at infrared and optical wavelengths. In the presence of refractivity fluctuations, interferometry at the longer infrared wavelengths enables larger apertures than those practical at optical wavelengths. On the other hand, two-color methods at optical wavelengths may help to reduce atmospheric effects [2]. Data from the ISI have already helped to characterize the Mt. Wilson atmosphere, as will be discussed in Section III. Descriptions of Mt. Wilson atmospheric behavior may well apply to other mountain-top astronomical sites.

In addition to the description of atmospheric fluctuation errors, tracking the trajectories of asteroids is another potential application of infrared interferometry in the DSN. Asteroid astrometry benefits both reference frame development and science [3]. Figure 1 shows the approximate flux of an asteroid located at 1 astronomical unit (AU) from the Sun. Various simplifications regarding the angular distribution of thermal flux from the asteroid make the figure approximate at the 30-percent level, but the illustrated wavelength dependence of the radiation is much better than that. The figure applies to the two cases noted, a 10-km-diam asteroid at 0.05 AU from the Earth or a 200-km-diam asteroid at 1 AU from the Earth. The ISI operates at 11 μm and, with recent sensitivity upgrades, should be able to make astrometric measurements of objects with flux in the 1000-Jy range. Optical or infrared measurements of GPS satellites will help to locate the asteroids in the radio VLBI frame used for angular spacecraft tracking. Astrometry of asteroid trajectories will also help to determine their masses [3].

Ground-based demonstrations with the ISI will suggest improvements to the infrared and optical astrometric techniques, as well as the nature of future space-based tracking systems. This article describes recent ISI data acquisition and analysis that help to establish an instrumental and atmospheric error budget. In the next section, the current instrumental characteristics of the ISI and the restrictions they impose on astrometric performance will be discussed. Section III shows characteristics of the Mt. Wilson atmosphere that must be addressed in future demonstrations, and Section IV describes the potential for upgrading both the instrumentation and analysis algorithms to achieve astrometry below the 50-nrad level.

II. Instrumental Sensitivity and Systematics

A single telescope of the ISI is shown in Fig. 2. Each of the two telescopes consists of a steerable flat mirror (on the right), a focusing parabolic mirror, optics, and electronics that detect the infrared signal and convert it to a 2-GHz-wide radio signal for cross-correlation. Helium-neon laser distance interferometers (HeNe LDI's) in each telescope monitor the path lengths between the flat and parabolic mirrors and behind the flat mirror to the optics table. The sensitivity of the ISI for infrared astrometry is limited by the noise in the output of the heterodyne receivers, which is about twice the quantum limit, or equivalent to a single-sideband system temperature of approximately 2600 K. An ISI interferometric time series for the star Alpha Orionis is shown in Fig. 3. These data were taken on September 8, 1992, on a 13-m baseline. There are points in the time series when a cycle may have been incorrectly assigned, but by and large the phase seems properly connected.

A general requirement on the sensitivity of astrometric devices is that the white (quantum or thermal) noise be low enough to allow short integration times as compared to those characteristic of appreciable propagation media effects. For interferometric devices, both white noise and low-frequency-peaked propagation noise [4,5] contributions to the phase must be small enough to allow

phase connection. Usually rms phase variations $\leq$0.1 cycle guarantee reliable phase connection. These qualitative statements are illustrated quantitatively in Fig. 4, which shows the point-to-point rms phase variation as a function of integration time for data taken from Fig. 3 and from Alpha Orionis on October 12, 1989. Between the two epochs shown in Fig. 4, a number of sensitivity enhancements were made, including the installation of an improved heterodyne detector in one telescope of the ISI. Low-frequency-peaked atmospheric effects increase as the integration interval increases. Quantum noise from the heterodyne detectors, on the other hand, is white or frequency independent and should therefore average and produce smaller rms phase variations with increased integration time. The decreasing trend with increasing integration times until about 0.2 sec is presumably due to quantum noise, while the increasing trend from 0.2 sec on is associated with atmospheric refractivity fluctuations. The minimum rms phase fluctuation—i.e., the point at which the system noise and atmospheric trends cross—determines the optimal integration time. As can be seen from the figure, sensitivitity upgrades improve performance by lowering the point-to-point fluctuation associated with the optimal integration time between about 0.2 and 0.13 cycle. If there were no rise in Fig. 4 due to atmospheric fluctuations, then integration times could be extended indefinitely and poor sensitivity could be tolerated. During nights of excellent seeing, for example on October 10, 1989, integration times of 1 sec or more were used to connect phase. Figure 4 thus illustrates the relationship between sensitivity and atmospheric fluctuations. Based on Fig. 4, "good seeing" will be defined from here on as atmospheric phase fluctuations less than 0.1 infrared cycle on 0.2-sec time scales. Reliable phase connection requires slightly better sensitivity than that evidenced in Fig. 4 for typical Mt. Wilson observing conditions. Future hardware upgrades, including installation of a new heterodyne detector in the other telescope of the ISI, should improve the potential for phase connection and therefore for infrared astrometry.

In addition to ISI sensitivity, systematic instrumental effects were studied by examining HeNe LDI path delay time series. They revealed resonances that may originate from the movement of the telescopes while tracking, or from resonances in the power supply. The resonances were at about 7 Hz, but sometimes multiple resonances between 1 and 10 Hz were found. The amplitudes of those resonances are such that they just barely contribute to infrared phase instability, but because they occur at frequencies which might cause additional problems with phase connection, we will attempt to identify and minimize them when analyzing data taken this past summer and fall.

III. Atmospheric Limitations in Current ISI Astrometric Demonstrations

The discussion of atmospheric errors in this section assumes that phase-connection problems will be solved by improved ISI sensitivity, as mentioned above. With reliable phase connection, the atmosphere still limits astrometric accuracy by causing different path-length changes between the two telescopes of the ISI. This section discusses the optimal use of HeNe LDI data to minimize atmospheric effects and the altitude dependence of the fluctuations as derived from model calculations.

In Fig. 5, the Alpha Orionis data from September 8, 1992, are shown again, plotted with the telescope-differenced HeNe LDI path lengths, scaled to infrared cycles, and multiplied by three to demonstrate the approximate 0.6 correlation. This correlation suggests that simple subtraction of the telescope-differenced HeNe LDI path delays from the interferometric delays is suboptimal [4]. The time series in Fig. 5 prompted a model calculation to explore the optimal utilization of the HeNe LDI data in the astrometric analysis and to assess the resulting astrometric accuracy. A calculation of the expected level of correlation between HeNe LDI and interferometric path delays was performed using the formalism of [5], and implemented with the numerical techniques of [6]. The total interferometric path length due to nonzero tropospheric refractivity $\tau_{trop}(\theta,\phi,t)$ at elevation angle θ, azimuth ϕ relative to the orientation of the ISI trailers, and time t is given by

$$\tau_{trop}(\theta,\phi,t) \;=\; \tau_{atm}(\theta,\phi,t) \;+\; 2\tau_{HeNe}(t) \qquad (1)$$

where $\tau_{atm}(\theta,\phi,t)$ is the contribution to the interferometric path delay from the differences in atmospheric refractivity along the electromagnetic paths from the observed object to each of the two telescopes of the ISI, and $\tau_{HeNe}(t)$ is the ground-based, one-way, telescope-differenced HeNe LDI path delay due to nonzero refractivity. The HeNe LDI path lengths are defined to lie along the x-axis at $(\theta,\phi) = (0,0)$. The factor of 2 in Eq. (1) accounts for the double traversal of the HeNe LDI path by the infrared interferometric signal: once from the flat mirror to the parabola (propagating to the left in Fig. 2) and once from the parabola through the cat's eye to the optics table in back of the flat mirror (propagating to the right in Fig. 2).

The atmospheric and HeNe LDI path delay terms in Eq. (1) are

$$\tau_{atm}(\theta,\phi,t) = \frac{1}{c\sin\theta}\int_0^h [\chi(\vec{r}_{2,atm}(\theta,\phi,z,t)) - \chi(\vec{r}_{1,atm}(\theta,\phi,z,t))]dz$$

$$\tau_{HeNe}(t) = \frac{1}{c}\int_0^l [\chi(\vec{r}_{2,HeNe}(x)) - \chi(\vec{r}_{1,HeNe}(x))]dx \quad (2)$$

where $\chi(\vec{r}_{i,atm})$ is the refractivity at the point denoted by the vector $\vec{r}_{i,atm}$ along the line of sight at height z above the ith telescope. For the HeNe LDI delay, $\chi(\vec{r}_{i,HeNe}(x))$ is the refractivity at the vector position a distance x along the HeNe path for the ith telescope. In Eq. (2), h is the height of the turbulent atmosphere, l is the length of the HeNe LDI path (which is 5 m), and c is the speed of light in a vacuum. Using these expressions, the correlation ρ plotted in Fig. 6 is

$$\rho = \frac{<\tau_{trop}\tau_{HeNe}>}{\sqrt{<\tau_{trop}^2><\tau_{HeNe}^2>}} \quad (3)$$

where <> means ensemble average. The abscissa of Fig. 6 is h in Eq. (2). The ensemble averages of refractivity were evaluated using Kolmogorov–Taylor structure functions as in [5], with a structure constant of $4 \times 10^{-7} m^{-1/3}$, an atmospheric height of 25 m, a wind speed of 1 m/sec, and a saturation scale of 10 m. These parameters were chosen because they produce temporal structure functions similar to those of the data of Fig. 5. The line-of-sight coordinates (θ,ϕ) = (37.6, 71 deg) were taken from the data of Fig. 5, and the horizontal line in Fig. 6 is ρ derived from the data of Fig. 5, assuming that a temporal average of ρ over a single scan is equal to an ensemble average over many scans (ergodicity). From Fig. 6, a 25-m height is inferred for the turbulent atmosphere. This is a model-dependent result, and the sensitivity of the result to departures from the Kolmogorov–Taylor assumptions will be discussed in future articles.

The above atmospheric modelling can be used to construct an optimal least-squares estimator for the interferometric delay at the middle of an observation interval, which is the fundamental quantity of astrometric interest. The observed interferometric delay is modelled as

$$\tau_{int}(\theta,\phi,t) = \tau_0(\theta,\phi,t_0) + (t-t_0)\dot{\tau}(\theta,\phi,t_0) + \tau_{trop}(\theta,\phi,t) \quad (4)$$

where $\tau_0(t_0)$ is the delay at the reference time t_0, and the changes in θ and ϕ due to sidereal tracking have been ignored. The τ_0 delay and the linear delay rate $\dot{\tau}$ include contributions due to baseline and celestial source coordinates that differ from those used in the lobe rotator model of the ISI correlator. An optimal estimator for τ_0 can be formed [7], and its error standard deviation calculated using the covariance of τ_{trop} between all times t_i and t_j, which, suppressing the θ and ϕ arguments, is given by

$$\mathrm{cov}\,(\tau_{\mathrm{trop}}(\mathrm{t_i}), \tau_{\mathrm{trop}}(\mathrm{t_j})) = <\tau_{trop}(t_i)\tau_{trop}(t_j)> - <\tau_{trop}(t_i)><\tau_{trop}(t_j)> \quad (5)$$

The two ensemble averages in the second term on the right of Eq. (5) are nearly zero for an interferometer with both telescopes at the same site. Again, the formalism of [5] can be used to evaluate the ensemble averages that result after inserting expressions from Eq. (2) into the first term on the right of Eq. (5). Figure 7 shows the calculated, troposphere-limited, error standard deviation for angular astrometry, which is c/B times the standard deviation for τ_0 for a 13-m baseline length B as a function of scan integration time. The upper curve shows the effect of the refractivity fluctuations in the absence of HeNe LDI calibration, and the lower curve shows the improvement if the current HeNe LDI calibrations are optimally used. For 1000-sec scans, an approximate 100-nrad accuracy seems attainable for interferometry with optimal HeNe LDI calibration. For azimuths along the HeNe LDI path, the HeNe LDI-calibrated accuracy is improved by about 20 percent.

It should be noted that estimation procedures, which are calculationally simpler that the optimal procedure described above, may be used in actual data analysis; a negligible loss in astrometric accuracy may result. The formulation using Eqs. 1–5 was presented to give insight into the turbulent atmospheric distance scales, the nature of ρ, and the reduction in astrometric error using HeNe LDI calibration.

In addition to the optimal analysis of the HeNe LDI and interferometric path delays, the results of Fig. 6 suggest that local measurements of refractivity in the first 25 m of the atmosphere may yield better than 100-nrad astrometry for observations when the HeNe LDI correlation is high. These local measurements could be meteorological or could consist of additional HeNe LDI's that sample the vertical paths above the ISI. It is very important to note that the

above approaches, which exploit the high correlation between the HeNe LDI and atmospheric path delays, may have limited utility. On many nights in the fall of 1992, with poorer seeing than that of September 8, 1992, HeNe LDI fluctuation levels not much different from those of Fig. 5 were observed, while the interferometric fluctuations were much larger than those of Fig. 5. Because the large fluctuations prevented reliable interferometric phase connection on those nights, the width of the power spectrum of the fringe amplitudes coming from the ISI correlator was used as the measure of the fluctuation level. The fact that the interferometer signal was correlated with the HeNe LDI delays on nights of good seeing and much less so on nights of poorer seeing suggests the following picture characterizing the Mt. Wilson atmosphere: During relatively good seeing, the atmospheric fluctuations are fairly low to the ground (within the first 25 m) and optimal incorporation of HeNe LDI data and/or other ground-based calibration strategies may yield 100-nrad-or-better infrared astrometry. During poor seeing, atmospheric fluctuations occur much higher than 25 m above the ISI and neither HeNe LDI data nor ground-based calibration schemes will be of much help. In that case, laser guide star technology [8] may be of use. This hypothesis is consistent with the picture of the atmosphere in [4], in which larger lateral saturation scales are attributed to nights of poorer seeing. The validity of this description of the atmosphere above Mt. Wilson and the ultimate astrometric accuracy of the ISI will be explored with data taken in the summer and fall of 1993.

IV. Summary and Future Directions

Applications of infrared astrometry to DSN tracking include research into techniques for tracking infrared or optical space-borne lasers, reference frame development, and astrometric science at infrared or optical wavelengths. The commonality of atmospheric problems at infrared and optical wavelengths and the capability of larger apertures at infrared wavelengths make infrared interferometry a good tool for studying atmospheric astrometric limitations. Asteroid astrometry and the measurement of gravitational deflection close to the Sun are examples of reference frame development and science that may be enabled by infrared interferometry in the DSN.

By comparing astrometric data from 1989 and 1992, we have verified that instrumental upgrades have indeed improved interferometric phase determination at short time scales. The point-to-point phase scatter on 0.2-sec time scales is about 0.13 infrared cycle for good seeing conditions. A factor of 2 improvement in the point-to-point phase scatter would greatly increase the reliability of interferometric phase connection. This factor of 2 may be realized with additional hardware sensitivity upgrades. Resonances have also been identified in the instrumental HeNe LDI calibration path lengths. These resonances are mainly at 7 Hz and are just barely strong enough to affect the infrared astrometric phase.

Analysis and modelling of ISI data taken in the fall of 1992 suggest a two-component model for the turbulent atmosphere above Mt. Wilson. For good seeing conditions, a 25-m turbulent atmospheric height has been inferred, based on the correlation between HeNe LDI and interferometric path-length fluctuations. A small saturation scale of 10 m was also inferred from the ISI data for good seeing. For poorer seeing conditions, the HeNe LDI–interferometric correlation is weaker, suggesting that the turbulent atmosphere has substantial components above 25 m. This modelling was also used to determine that the atmosphere-limited astrometric accuracy on an ISI 13-m baseline during good seeing, with optimal HeNe LDI calibration, was about 100 nrad for a 1000-sec scan. Accuracy at this level would be a factor of 4 better than previous infrared astrometric results [9]. This level of astrometric accuracy has yet to be demonstrated on multiple sources with the ISI. Single-source phase traces and atmospheric modelling have been used to infer the potential accuracy of the ISI.

Reliable phase connection, optimal application of HeNe LDI calibration, and the resulting 100-nrad single-source astrometry will be demonstrated with data taken in the next observing season. Multiple-source astrometry will also be attempted. This will require developing acquisition or analysis techniques to resolve cycle ambiguities between observations of multiple sources. Future astrometric improvements may include local monitoring of atmospheric effects to improve accuracy on nights of good seeing. Such monitoring could involve a combination of meteorological sensors and new HeNe LDI paths. In the more distant future, the development of an infrared reference frame and asteroid astrometry will be pursued. A direct-detection (as opposed to heterodyne) system is being considered for the ISI on 5-year time scales. Direct detection would greatly increase the usable ISI bandwidth and sensitivity, enabling astrometry in a much wider variety of seeing conditions.

It should be noted that because of the apparent small saturation scale during periods of good seeing, increases in baseline length will yield almost proportionate improvements in accuracy. Data taken on azimuths closer to that of the HeNe LDI will be more effectively calibrated by op-

timal application of HeNe LDI data. Considering these factors, astrometric accuracy of the order of 50–100 nrad is probably characteristic of future ISI single-observation performance in the absence of the above-mentioned meteorological calibrations. Because of the small saturation scales, troposphere-induced errors for observations from the same session, or from different sessions, should be uncorrelated. By averaging results over many observations, astrometric accuracies of much better than 50–100 nrad should be possible.

References

[1] J. R. Lesh, L. J. Deutsch, and W. J. Weber, "A Plan for the Development and Demonstration of Optical Communications for Deep Space," *The Telecommunications and Data Acquisition Progress Report 42-103, vol. July–September 1990*, Jet Propulsion Laboratory, Pasadena, California, pp. 97–109, November 15, 1990.

[2] M. Colavita, M. Shao, and D. H. Staelin, "Two-Color Method for Optical Astrometry: Theory and Preliminary Measurements with the Mark III Stellar Interferometer," *Applied Optics*, vol. 26, pp. 4113–4122, 1987.

[3] M. Hoffmann, "Asteroid Mass Determination: Present Situation and Perspectives," in *Asteroids II*, edited by R. P. Binzel, T. Gehrels, and M. S. Matthews, Tucson: University of Arizona Press, pp. 228–239, 1989.

[4] M. Bester, W. C. Danchi, C. G. Degiacomi, L. J. Greenhill, and C. H. Townes, "Atmospheric Fluctuations: Empirical Structure Functions and Projected Performance of Future Instruments," *Ap. J.*, vol. 392, p. 357, 1992.

[5] R. N. Treuhaft and G. E. Lanyi, "The Effect of the Dynamic Wet Troposphere on Radio Interferometric Measurements," *Radio Science*, vol. 22, p. 251, 1987.

[6] G. J. Bierman, *Factorization Methods for Discrete Sequential Estimation*, Orlando: Academic Press, 1977.

[7] W. C. Hamilton, *Statistics in Physical Science*, New York: Ronald Press, 1964.

[8] R. K. Tyson, *Principles of Adaptive Optics*, Boston: Academic Press, Inc., 1991.

[9] E. C. Sutton, S. Subranmanian, and C. H. Townes, *Astronomy Astrophysics*, vol. 110, pp. 324–331, 1982.

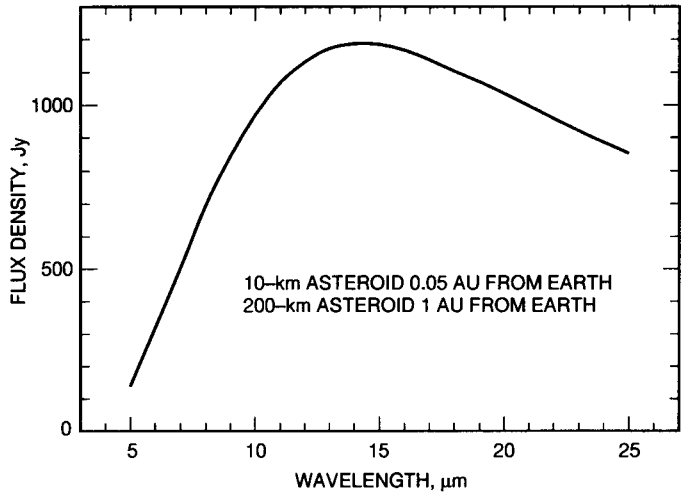

Fig. 1. Black-body calculation of approximate flux density for an asteroid located 1 AU from the Sun, as a function of wavelength.

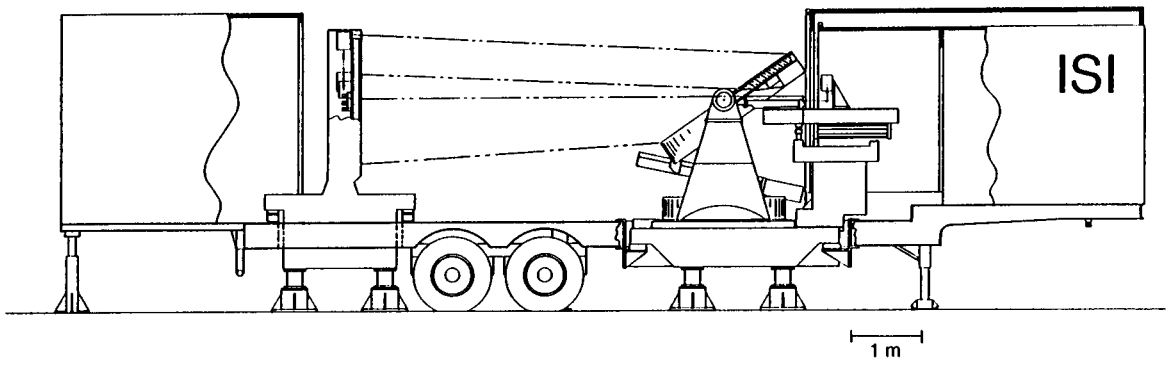

Fig. 2. A single telescope of the ISI, showing the flat mirror, parabolic mirror, and optics table.

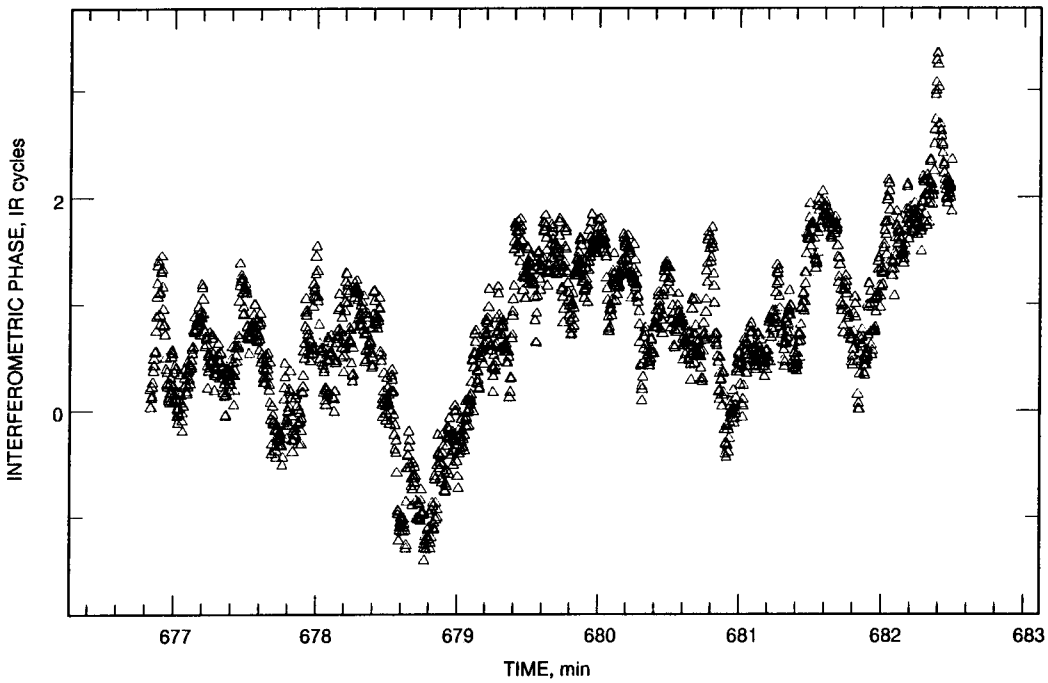

Fig. 3. Infrared interferometric phase as a function of time for the star Alpha Orionis on September 8, 1992.

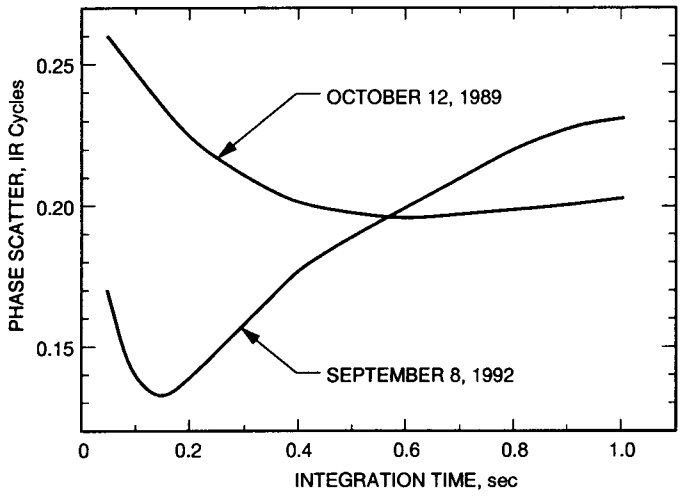

Fig. 4. The point-to-point rms phase scatter as a function of integration time for the data of Fig. 3.

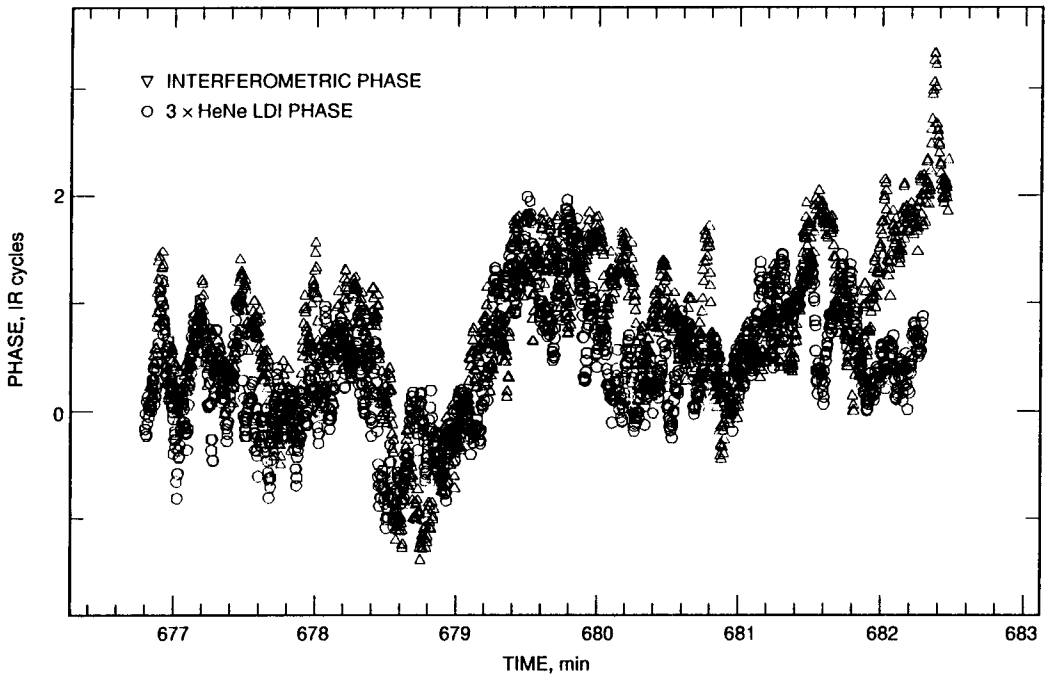

Fig. 5. The phase time series of Fig. 3 with HeNe LDI phases, scaled to infrared cycles, differenced between telescopes, and multiplied by 3.

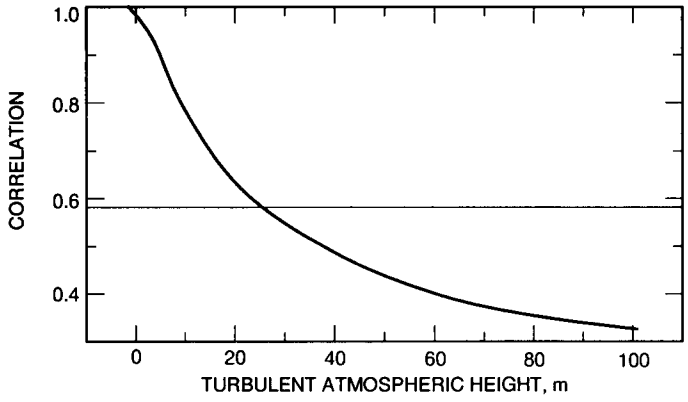

Fig. 6. The calculated correlation between telescope-differenced HeNe LDI data and interferometric data for the conditions of the data in Figs. 3–5. The horizontal line is the actual correlation from the data of Fig. 5.

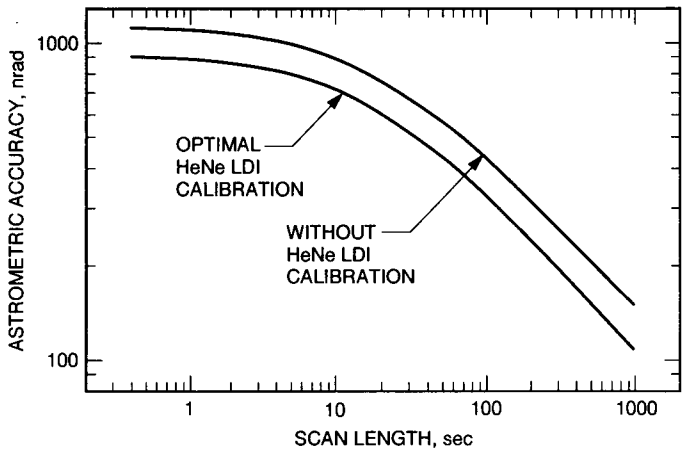

Fig. 7. The calculated astrometric accuracy, as a function of scan length, with and without optimal HeNe LDI calibration, for the conditions of Figs. 3–5.